



Cite this: *Mol. Syst. Des. Eng.*, 2018, 3, 723

Received 12th June 2018,  
Accepted 6th September 2018

DOI: 10.1039/c8me00035b

rsc.li/molecular-engineering

Here we present successful surface passivation of halide perovskite nanowires with anodic aluminum oxide templates. The  $\text{CH}_3\text{NH}_3\text{PbBr}_3/\text{alumina}$  nanowires have charge carrier lifetimes of more than 20 ns and a remarkably low surface recombination velocity of  $37.2 \pm 20 \text{ cm s}^{-1}$ . The ease of their fabrication and their excellent photophysical properties make them a promising candidate for integration in optoelectronic device structures.

Shockley–Read–Hall (SRH) surface and bulk recombination is detrimental to the performance of semiconductor-based devices, especially at low charge carrier injection levels.<sup>1</sup> Thus, for high-efficiency devices, strategies mitigating the influence of those defects must be developed, with varying requirements for bulk and surface defects. Hybrid halide perovskites are not an exception to this rule, as their efficient performance is tightly bound to tackling the right approaches for identifying and confronting their defects. Their unusual defect chemistry and physics have enabled the rapid and simple fabrication of high-quality absorbers and emitters with long charge-carrier diffusion lengths and lifetimes, high absorption coefficients and high emission yields.<sup>2–4</sup> Those photophysical properties in turn depend directly on the charge carrier generation and recombination dynamics. Thus, it is crucial to provide in-depth understanding of how fast and *via* which channels the charge carriers recombine within the perovskite light-absorber. This knowledge assists in developing strategies to minimize the structural imperfections, such as bulk and surface lattice defects for designing highly efficient optoelectronic devices. Interfacial defects facilitate the charge

## Surface recombination velocity of methylammonium lead bromide nanowires in anodic aluminium oxide templates†

Parisa Khoram,<sup>a</sup> Sebastian Z. Oener,<sup>ab</sup> Qianpeng Zhang,<sup>c</sup> Zhiyong Fan<sup>c</sup> and Erik C. Garnett<sup>\*,a</sup>

### Design, System, Application

Semiconductor nanowires have been designed in the past few years as building blocks of efficient optoelectronic devices. Their 1-dimensional geometry and high surface-to-volume ratio also make them perfect systems for studying several geometry-related properties of semiconductors. Recently, enormous attention has been devoted to hybrid halide perovskite semiconductors due to the ease of their fabrication, as well as their high device efficiency. Perovskite/metal oxide interfaces are an inevitable part of these devices, acting as a source of charge recombination, and decreasing the performance of the device. Therefore, it is crucial to study the charge carrier recombination processes at these interfaces and quantify them. Halide perovskite nanowires embedded in anodized aluminum oxide provide a well-controlled platform to study the charge carrier dynamics and effect of surface passivation with alumina. These  $\text{CH}_3\text{NH}_3\text{PbBr}_3/\text{alumina}$  nanowires have high charge carrier lifetimes of more than 20 ns. We use the diameter-dependent charge carrier lifetimes to extract a remarkably low surface recombination velocity (SRV) of  $37.2 \pm 20 \text{ cm s}^{-1}$  for the perovskite/alumina interface, which confirms the passivating role of alumina. Due to the ease of their fabrication and their excellent photophysical properties, the perovskite/alumina nanowires can be considered as a candidate for optoelectronic device structures.

recombination processes and impact the overall performance of the device negatively.<sup>5</sup>

Passivating the surfaces of traditional inorganic semiconductors such as Si was a milestone in achieving highly efficient solar cells.<sup>6</sup> In halide perovskites, similar passivation methods have been investigated by incorporation of external materials as well as new approaches according to their special chemical structure, such as self-formation of  $\text{PbI}_2$  on  $\text{CH}_3\text{NH}_3\text{I}_3$  thin films through ambient exposure.<sup>7–9</sup> Surfaces, interfaces or grain boundaries of halide perovskites have been passivated using chemical treatments *via* halogenated organic compounds,<sup>10</sup> Lewis bases,<sup>11</sup> fullerene,<sup>12–15</sup> graphene<sup>16</sup> and potassium.<sup>17</sup> Many research groups investigated the application of ultra-thin metal oxide films, such as  $\text{ZnO}$ ,<sup>18–21</sup>  $\text{SnO}_x$ <sup>20</sup> and  $\text{Al}_2\text{O}_3$ <sup>19,21–26</sup> by atomic layer deposition (ALD) as passivation layers in halide perovskite solar cells. Note that this is different than the common use of ALD metal oxides as carrier-selective charge

<sup>a</sup> Center for Nanophotovoltaics, AMOLF, Science Park 104, 1098 XG Amsterdam, The Netherlands. E-mail: garnett@amolf.nl

<sup>b</sup> Department of Chemistry and Biochemistry, University of Oregon, Eugene, Oregon 97403, USA

<sup>c</sup> Department of Electronic and Computer Engineering, The Hong Kong University of Science and Technology, Clear Water Bay, Kowloon, Hong Kong SAR, China

† Electronic supplementary information (ESI) available. See DOI: 10.1039/c8me00035b

‡ These authors contributed equally.

transfer layers in planar perovskite solar cells.<sup>27</sup> In most of the surface passivation studies, the addition of an oxide layer improved the device performance and stability. However, little is known about the charge carrier dynamics at the perovskite/metal oxide interfaces and in particular the recombination rates and SRV have not been quantified at these interfaces.

Nanowires are promising geometries for applications in electronic and optoelectronic devices<sup>28–30</sup> and also for case studies of dimension-dependent properties. Previously, semiconductor nanowires such as Ge,<sup>31</sup> Si<sup>32,33</sup> and InP<sup>34</sup> were studied to quantify the dynamics of charge carriers and/or investigate the effects of surface passivation. By controlling their surface to volume ratio, they provide a versatile platform to manage and quantify the contribution of surface and bulk precisely. In the past few years, perovskite nanowires have been realized *via* various solution<sup>35</sup> and vapour-based methods.<sup>36,37</sup> Among those, perovskite nanowires embedded in anodic aluminum oxide (AAO) templates have been successfully incorporated in efficient solar cells<sup>38</sup> and photodetector devices,<sup>39,40</sup> demonstrating the high potential of perovskite nanowires wrapped with alumina (perovskite/alumina) for future applications.

Here we study the recombination dynamics at the perovskite/alumina interface using perovskite nanowires embedded in anodic aluminum oxide (AAO) templates. The nanowires are fabricated by applying a pressure gradient across a template coated with a viscous halide perovskite precursor solution, similar to the extrusion technique we introduced previously.<sup>41</sup> Fabrication from the perovskite solution directly into the AAO template avoids the exposure of the water-sensitive perovskite surface to the water precursor in a typical Al<sub>2</sub>O<sub>3</sub>-ALD process. By using templates with various pore sizes from ~150 to ~350 nm, we systematically change the surface-to-volume ratio of the final CH<sub>3</sub>NH<sub>3</sub>PbBr<sub>3</sub> perovskite nanowires. Assuming that the bulk quality and radiative recombination rates stay constant, the changes in total recombination rates should be directly connected to the recombination at the perovskite nanowire surfaces. Time-resolved PL (TRPL) spectroscopy is used to obtain the dynamics of photoexcited carriers in the perovskite nanowire arrays. The recombination rates are extracted by fitting the PL intensity decay to a rate equation that includes radiative and non-radiative recombination. The obtained lifetime increases slightly from 24.3 ± 2.3 ns to 28.3 ± 1.5 ns when increasing the diameter by more than a factor of two. This shows the weak dependence of the PL lifetime on the nanowire diameter, suggesting a very low surface recombination velocity (SRV). By fitting these TRPL results to a simple recombination model, we extract an SRV of 37.2 ± 20 cm s<sup>-1</sup>, indeed much lower than the value measured for unpassivated surfaces of single crystal CH<sub>3</sub>NH<sub>3</sub>PbBr<sub>3</sub> perovskites (~10<sup>3</sup> cm s<sup>-1</sup>).<sup>42–44</sup> These results indicate that alumina provides excellent passivation for CH<sub>3</sub>NH<sub>3</sub>PbBr<sub>3</sub> perovskite nanowires. This structure can be extended to incorporation into future devices.<sup>38–40</sup>

To fabricate the perovskite/alumina nanowires, we employed a differential-pressure-driven process similar to the

extrusion method introduced previously.<sup>41</sup> However, when the perovskite solution inside the AAO pores reaches the AAO top surface, the process is terminated (before nanowire extrusion), as schematically shown in Fig. 1a. The perovskite solution fills the nanopores of the AAO template and evaporation of the solvent leaves the perovskite/alumina nanowires inside the AAO pores. Fig. 1b shows the SEM image from the bottom surface of the template prior to filling with perovskite, whereas the SEM image in Fig. 1c indicates the filling of the pores after the application of a pressure gradient. Conductivity measurements (Fig. S1†) and cross-sectional SEM images (Fig. S2†) of the filled AAO templates show that the perovskite is extended through a large fraction of the AAO pores (see the ESI†). This simple method provides highly ordered arrays of perovskite nanowires with tuneable lengths (determined by the AAO thickness) embedded in a transparent medium with high surface passivation potential.

The optical properties of the perovskite/alumina nanowires are characterized with steady-state PL (405 nm excitation) and absorption measurements (Fig. 2a). The emission peak at 540 nm (2.29 eV) matches the band gap of CH<sub>3</sub>NH<sub>3</sub>PbBr<sub>3</sub>. The nanowire arrays with different diameters, but the same length (50 μm), have similar PL and absorption spectra. Finite-difference time-domain (FDTD) simulations are performed to study the light intensity distribution and absorption in perovskite/alumina nanowire arrays with various diameters, as presented in Fig. S4.† The electric-field intensity ( $|E|^2$ ) upon excitation with short-wavelength light (485 nm) decays quickly within the first 5 nanometers away from the surface for all the nanowire arrays with different diameters. The simulated absorption spectrum is in agreement with the experimental absorption data shown in Fig. 2a.

We used three templates with average pore diameters of 150.4 ± 35.7, 208.2 ± 34.8 and 361.7 ± 20.4 nm and filled them with CH<sub>3</sub>NH<sub>3</sub>PbBr<sub>3</sub> nanowires to study the charge

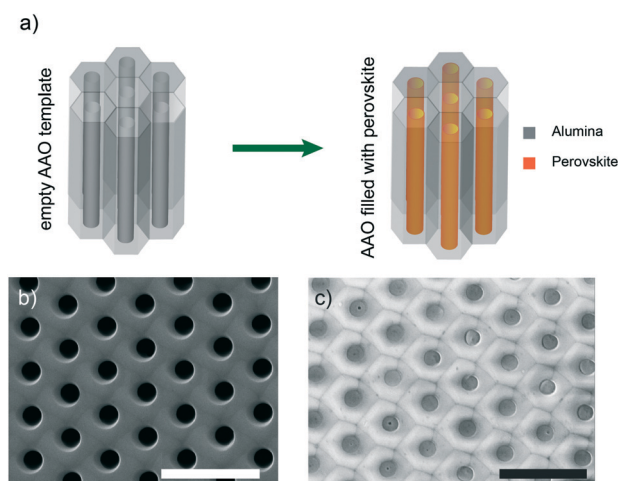
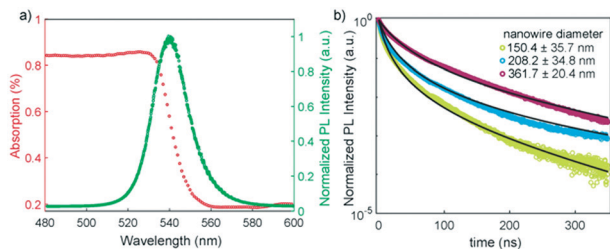


Fig. 1 CH<sub>3</sub>NH<sub>3</sub>PbBr<sub>3</sub> nanowires embedded in the AAO template. a) Schematic of the AAO template before and after filling with the perovskite solution. b) SEM images of the bottom side of the template before and c) after the pores were filled with the solution. The scale bars correspond to 2 μm.



**Fig. 2** Steady-state PL, absorption and transient PL of perovskite/alumina nanowire arrays. a) PL (405 nm excitation) and absorption spectra of the nanowire arrays with an average diameter of 361.7 nm. The samples with a smaller diameter had similar absorption and PL spectra, as shown in the ESI† b) PL intensity decay of nanowire arrays with various diameters. The black line shows the fit to the data according to eqn (3).

carrier dynamics and the contribution of the perovskite/alumina interface in the recombination mechanism. By decreasing the nanowire diameter and keeping the bulk recombination constant, we increase the relative contribution of the surface to the overall recombination process. Since all the samples were prepared from the same solution batch at the same time, and also measured at the same time, we expect the bulk quality and defect densities to be comparable for all of them. Therefore, changing nanowire diameters would affect the non-radiative recombination because of the higher density of trap states on the surface. Here we assume that there is no radiative channel in trap-assisted recombination and the only radiative process leading to emission is the bimolecular recombination of two charge carriers.<sup>45</sup> Therefore, the decay of PL as a function of time can be written as:

$$PL(t) = Ak_2n(t)^2 + b \text{c}g \quad (1)$$

where  $A$  is the collection efficiency,  $n(t)$  is the charge carrier density as a function of time and  $b \text{c}g$  is the background. Here,  $k_2$  is the bimolecular recombination rate coefficient defined *via* the decay of charge carriers over time, as formulated below:

$$\frac{dn(t)}{dt} = -k_3n(t)^3 - k_2n(t)^2 - k_1n(t) \quad (2)$$

where  $k_1$  is the recombination rate coefficient associated with the monomolecular trap-assisted recombination and  $k_3$  is the Auger recombination rate coefficient.

We measured the  $PL(t)$  of the nanowire arrays with time-correlated single photon counting (TCSPC) over more than 8 different spots on each sample (details in the ESI†). A blue laser (485 nm) with a fluence of  $8.3 \mu\text{J cm}^{-2}$  excited the samples and generated an initial charge carrier density of  $3.2 \times 10^{17} \text{ cm}^{-3}$ . The calculation of carrier density is explained in detail in the ESI†. At this carrier density, the role of Auger recombination is considered negligible.<sup>45,46</sup> The representative PL decay curves of each sample are shown in Fig. 2b. We solved eqn (2) for  $n(t)$ , disregarding the Auger term, and inserted the result in eqn (1):

$$PL(t) = Ak_2 \left( \frac{k_1n_0}{(k_1 + k_2n_0)\exp(k_1t) - k_2n_0} \right)^2 + b \text{c}g \quad (3)$$

where  $n_0$  is the initial carrier density at  $t = 0$  and  $k_1$  is the trap-assisted recombination coefficient.

Globally fitting of eqn (3) to the experimental TRPL data allows us to extract the trap-assisted and radiative recombination coefficients  $k_1$  and  $k_2$  as listed in Table 1. More details of the fitting procedure can be found in the ESI†.

As seen in Table 1, increasing the nanowire diameter enhances the lifetime of charge carriers. The changes in  $k_1$  can be attributed to the changes of surface defect density due to different surface contributions of each nanowire array, as well as sample-to-sample bulk defect density variations. Nevertheless, the decrease in  $k_1$  follows a trend with increasing nanowire diameter considering the error bars of the experiment. The variation of  $k_2$  from sample to sample is small, confirming that the radiative processes come from the materials' band structure and therefore depend on the materials' band structure and local density of states. The  $k_1$  values are in the same range as measured by Richter *et al.*<sup>47</sup> with transient absorption (TA) for  $\text{CH}_3\text{NH}_3\text{PbBr}_3$  thin films ( $2.5 \times 10^6 \text{ s}^{-1}$ ) and by Wu *et al.*<sup>44</sup> for  $\text{CH}_3\text{NH}_3\text{PbBr}_3$  single crystals with TRPL ( $2.9 \times 10^6 \text{ s}^{-1}$ ), but one order of magnitude lower than the values reported by Yang *et al.*<sup>46</sup> from TA measurements ( $2.7 \times 10^7 \text{ s}^{-1}$ ) for  $\text{CH}_3\text{NH}_3\text{PbBr}_3$  thin films. The radiative recombination coefficient is also comparable to the studies by Wu *et al.*<sup>44</sup> and Yang *et al.*<sup>46</sup> but  $\sim 10$  times lower than the reference reported by Richter *et al.*<sup>47</sup> Using the recombination coefficients, we calculated the charge carrier lifetime from eqn (4) as presented in the last column of Table 1.

$$\tau = \frac{1}{k_1 + k_2n} \quad (4)$$

The lifetime is relatively stable, increasing only slightly with diameter. Thus the relative surface contribution to the overall charge carrier recombination is small for the high surface passivation levels obtained here.

**Table 1** Recombination coefficients of  $\text{CH}_3\text{NH}_3\text{PbBr}_3$ /alumina nanowires with different diameters extracted from global fitting of eqn (3) to the measured PL decay, as shown in Fig. 2b. The average diameter of the nanowire ( $d$ ) was measured *via* SEM over  $\sim 40$  nanowires for each sample. The errors are standard deviations. Here,  $k_1$  is the trap-assisted recombination coefficient and  $k_2$  is the radiative recombination coefficient. The errors are standard errors of the mean of the extracted coefficients measured over more than 8 different spots for each sample. The charge carrier lifetime  $\tau$  is calculated from eqn (4) and the errors are standard error of the mean

$d$ (nm)	$k_1$ ( $\times 10^6 \text{ s}^{-1}$ )	$k_2$ ( $\times 10^{-10} \text{ cm}^3 \text{ s}^{-1}$ )	$\tau$ (ns)
$150.4 \pm 35.7$	$3.71 \pm 0.58$	$1.32 \pm 0.24$	$24.3 \pm 2.3$
$208.2 \pm 34.8$	$3.99 \pm 0.92$	$1.31 \pm 0.19$	$26.9 \pm 3.5$
$362.7 \pm 20.4$	$2.10 \pm 0.29$	$1.06 \pm 0.06$	$28.3 \pm 1.5$

In the long nanowires studied here, the diameter is essentially the identifier of the surface area to bulk volume. In order to discover the exact dependence of the recombination on the surface, we developed a model to relate the carrier lifetime to the nanowire diameter.

In the following, we assume a charge carrier diffusion length in  $\text{CH}_3\text{NH}_3\text{PbBr}_3$  that is larger than the radius of the nanowires<sup>25</sup> and hence a homogenous carrier concentration inside each individual nanowire and among all nanowires inside the laser spot. In this model, the surface recombination velocity is essentially a rate parameter that, together with bulk recombination, reduces the photo-generated carrier concentration observed *via* PL. Specific carrier gradients inside the nanowire, leading to complex carrier flow patterns are neglected. For a certain geometry, the total recombination is composed of two terms – bulk and surface – as shown below:

$$R_T = VR_B + AR_S \quad (5)$$

where  $R_T$  is the total recombination rate,  $V$  is the volume,  $A$  is the surface area, and  $R_B$  and  $R_S$  are the total recombination rates in the bulk per unit volume and at the surface per unit area. Considering the geometry of the nanowire as a cylinder with radius  $r$  and length  $l$ , the equation above can be written as:

$$R_T = \pi r^2 l (B + S_{\text{air}}/l) + 2\pi r (l S_{\text{alumina}}) \quad (6)$$

where  $B$  is the bulk recombination velocity,  $S_{\text{alumina}}$  and  $S_{\text{air}}$  are the rate at which the charge carrier move towards the nanowire interfaces (SRV) with alumina and air, respectively. Since  $B$  and  $S_{\text{air}}$  have the same dependence on the radius, we group them together as an effective bulk recombination term ( $R_v$ ). By dividing both sides of eqn (5) by  $\pi r^2 l$  (the nanowire volume), we end up with eqn (7), which allows us to extract  $S_{\text{alumina}}$  from the slope of the recombination rate *versus* the inverse of the nanowire radius:

$$R = R_v + \frac{2S}{r} \quad (7)$$

where  $R$  is the recombination rate per unit volume given by  $R(n, t) = k_2 n + k_1$  and by definition, is the inverse of the charge carrier lifetime ( $1/\tau$ ). Therefore, eqn (7) is rearranged in the final form:

$$\frac{1}{\tau} = R_v + \frac{2S}{r} \quad (8)$$

The inverse of the carrier lifetime is proportional to the inverse of the nanowire radius, where the slope of the line is  $2S$ , and the  $y$ -intercept is the effective bulk recombination rate. This model shows that the lower the slope is, the less the nanowire wall surface contributes to the recombination rate. Therefore, if a perfect passivation of the surface is provided, the line would be horizontal with slope zero, and re-

combination stemming only from the bulk and top surface. A similar approach using the continuity equation was implemented before by Léonard *et al.*<sup>31</sup> and Dan *et al.*<sup>33</sup> and the same linear relation of the recombination rate and nanowire diameter was derived, as also explained in the ESI.†

Fitting eqn (8) to the inverse of the average lifetimes (calculated from eqn (4) for more than 8 experiments for each sample) *versus* the inverse of the nanowire radius results in an SRV of  $37.2 \pm 20 \text{ cm s}^{-1}$  and a bulk recombination rate of  $3 \times 10^7 \text{ s}^{-1}$  at the initial carrier density of  $3.2 \times 10^{17} \text{ cm}^{-3}$  (Fig. 3a). The error is the standard deviation of SRV extracted from  $10^6$  linear fits of the averages of 5 randomly selected data points at each nanowire radius. This result shows that at this carrier density, the recombination is dominated by the bulk (with possible contributions from the top surface), and the side wall surface is well passivated. This value is considerably lower than SRVs reported in various studies for unpassivated  $\text{CH}_3\text{NH}_3\text{PbBr}_3$  single crystals<sup>43,44,48,49</sup> ( $1.6\text{--}6.7 \times 10^3 \text{ cm s}^{-1}$ ) and lower but in the same range as reported for the passivated surface of  $\text{CH}_3\text{NH}_3\text{PbBr}_3$  single crystals with UV- $\text{O}_3$  treatment ( $64 \text{ cm s}^{-1}$ ).<sup>48</sup> Fang *et al.*<sup>50</sup> reported an unusually low SRV of  $4 \text{ cm s}^{-1}$  for the  $\text{CH}_3\text{NH}_3\text{PbBr}_3$  single crystals by controlling the physisorption of oxygen and water molecules on their surface.

We should note that SRV is a facet-dependent parameter. While single crystals of  $\text{CH}_3\text{NH}_3\text{PbBr}_3$  have (100) facets because of their cubic structure, the nanowire walls have higher index facets. Fig. S3† shows the X-ray diffraction (XRD) pattern of the  $\text{CH}_3\text{NH}_3\text{PbBr}_3/\text{AAO}$  nanowires. The (100) diffraction peaks are more pronounced which indicates that the nanowires within the AAO pores are grown in the  $\langle 100 \rangle$  direction. This indicates that the nanowire side walls have higher index facets. Most semiconductor nanowires, such as Si<sup>33</sup> and Ge,<sup>31</sup> have SRVs 2–3 orders of magnitude higher than what is reported in this study. Obtaining the incredibly small SRV value of  $37.2 \pm 20 \text{ cm s}^{-1}$  for high index facets of perovskite nanowires confirms the good passivation that

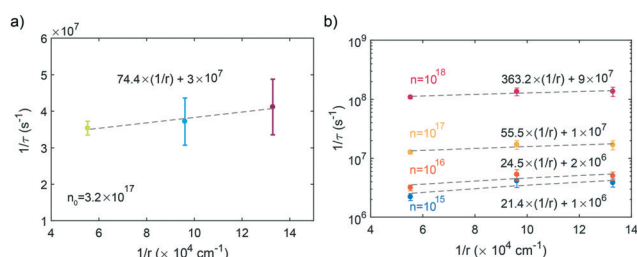


**Fig. 3** Modeling the surface recombination velocity (SRV) of perovskite/alumina using nanowires with various diameters. a) Recombination rate ( $1/\tau$ ) *versus* inverse of nanowire radii. The lifetime is calculated from eqn (4) for the initial carrier density as performed in the TRPL experiment. The dashed line shows the linear fit of eqn (8) to the experimental data. The equation achieved from the fit is written above the line. The slope is equal to  $2 \times \text{SRV}$  and the  $y$ -intercept is the effective bulk recombination. b) The estimation of SRV and total bulk recombination for various carrier densities from  $10^{15}$  to  $10^{18} \text{ cm}^{-3}$ . With increasing carrier density, SRV increases, but the effective bulk recombination stays dominant.

**Table 2** Surface ( $S$ ) and effective bulk ( $R_v$ ) recombination velocities for  $\text{CH}_3\text{NH}_3\text{PbBr}_3$ /alumina nanowires at different carrier densities.  $S$  and  $R_v$  are fit parameters, as shown in Fig. 3b.  $S/(R_v d_{\text{av}} + S)$  is the contribution of surface recombination to the total recombination for a representative nanowire with an average diameter of  $d_{\text{av}} = 200$  nm

$n$ ( $\text{cm}^{-3}$ )	$S$ ( $\text{cm s}^{-1}$ )	$R_v$ ( $\text{s}^{-1}$ )	$S/(R_v d_{\text{av}} + S)$ (%)
$10^{15}$	10.7	$10^6$	34.4
$10^{16}$	12.3	$2 \times 10^6$	23.5
$10^{17}$	27.7	$10^7$	12.2
$10^{18}$	182.2	$9 \times 10^7$	9.2

alumina provides. We reported previously<sup>41</sup> a slight deviation of the lattice constant from the theoretical value for a perfect cubic crystal structure in extruded  $\text{CH}_3\text{NH}_3\text{PbBr}_3$  nanowires. This might be due to the constrained growth environment of the perovskite nanowires within the AAO pores which may exist in  $\text{CH}_3\text{NH}_3\text{PbBr}_3$ /AAO nanowires as well. Further research is required to address the effects of constrained microstructures on the photo-physical properties of perovskite nanostructures.

The SRV depends not only on surface trap states (their type and density), but also on the charge carrier density.<sup>6</sup> Therefore, we expect an increase in SRV with increasing carrier density. We used the same recombination coefficients in Table 1, and plotted various total recombination lifetimes *versus* the nanowire radii in Fig. 3b for charge carrier densities of  $10^{15}$ – $10^{18}$   $\text{cm}^{-3}$ . A higher carrier concentration is not selected because of the increasing contribution of Auger recombination with higher intensities,<sup>51</sup> which is not included in our model. By fitting eqn (8) with the different carrier densities to the dependence of the lifetime on the nanowire radius, as shown in Fig. 3b, we obtained the respective surface and effective bulk as summarized in Table 2. The last column of this table shows that increasing the carrier density effectively makes the contribution of surface recombination to the total recombination rate ( $S/d + R_v$ ) smaller.

## Conclusions

In this study we fabricated long  $\text{CH}_3\text{NH}_3\text{PbBr}_3$  nanowire arrays embedded in AAO templates (perovskite/alumina nanowires) using a simple solution technique by suction of the perovskite solution through the AAO pores. The charge carrier recombination mechanism of the perovskite/alumina nanowire arrays was studied with time-resolved PL spectroscopy. Fitting of the PL intensity decay to a rate equation that includes radiative (bimolecular) and non-radiative (monomolecular) recombination was used to obtain the recombination rate coefficients. We estimated a charge carrier lifetime of more than 20 ns at the initial carrier density of  $3.2 \times 10^{17}$   $\text{cm}^{-3}$  for nanowires with various diameters. The inverse lifetimes increase linearly with decreasing nanowire diameter. This data was fitted to a model to extract a very low SRV of  $37.2 \pm 20$   $\text{cm s}^{-1}$  at the  $\text{CH}_3\text{NH}_3\text{PbBr}_3$ /alumina interface. The low SRV of passivated nanowires in comparison with that of

unpassivated  $\text{CH}_3\text{NH}_3\text{PbBr}_3$  single crystals ( $\sim 10^3$   $\text{cm s}^{-1}$ )<sup>44,49,52</sup> ensures that despite the large surface of perovskite nanowires, their surface was not dominant in recombination processes.

The presented results here confirm the passivation effect alumina provides for hybrid halide perovskites and quantify the surface recombination velocity at the perovskite/alumina interface for the first time. This study presents a simple systematic method for the passivation of perovskite surfaces, without the need for ALD deposition of  $\text{Al}_2\text{O}_3$ . Further studies to compare the perovskite nanowires passivated with ALD and the ones embedded in AAO templates will provide a comprehensive picture of the similarities and differences of these two methods.

## Conflicts of interest

There are no conflicts to declare.

## Acknowledgements

This work was done at AMOLF and partially supported by the Netherlands Foundation for Scientific Research (NWO) as well as the European Research Council (Grant Agreement No. 337328). The work in the Hong Kong University of Science and Technology was supported by the General Research Fund (project 16237816) from the Hong Kong Research Grant Council, and the National Natural Science Foundation of China (project 51672231).

## Notes and references

- W. Shockley and W. T. Read, *Phys. Rev.*, 1952, **87**, 835–842.
- M. a. Green, A. Ho-Baillie and H. J. Snaith, *Nat. Photonics*, 2014, **8**, 506–514.
- S. D. Stranks and H. J. Snaith, *Nat. Nanotechnol.*, 2015, **10**, 391–402.
- H. Wang and D. H. Kim, *Chem. Soc. Rev.*, 2017, **46**, 5204–5236.
- J. Shi, X. Xu, D. Li and Q. Meng, *Small*, 2015, **11**, 2472–2486.
- A. G. Aberle, *Progr. Photovolt.: Res. Appl.*, 2000, **8**, 473–487.
- L. Wang, C. McCleese, A. Kovalsky, Y. Zhao and C. Burda, *J. Am. Chem. Soc.*, 2014, **136**, 12205–12208.
- Q. Chen, H. Zhou, T. Song, S. Luo and Z. Hong, *Nano Lett.*, 2014, **14**, 4158–4163.
- T. J. Jacobsson, J.-P. Correa-Baena, E. Halvani Anaraki, B. Philippe, S. D. Stranks, M. E. F. Bouduban, W. Tress, K. Schenk, J. Teuscher, J.-E. Moser, H. Rensmo and A. Hagfeldt, *J. Am. Chem. Soc.*, 2016, **138**, 10331–10343.
- A. Abate, M. Saliba, D. J. Hollman, S. D. Stranks, K. Wojciechowski, R. Avolio, G. Grancini, A. Petrozza and H. J. Snaith, *Nano Lett.*, 2014, **14**, 3247–3254.
- N. K. Noel, A. Abate, S. D. Stranks, E. S. Parrott, V. M. Burlakov, A. Goriely and H. J. Snaith, *ACS Nano*, 2014, **8**, 9815–9821.
- K. Wojciechowski, S. D. Stranks, A. Abate, G. Sadoughi, A. Sadhanala, N. Kopidakis, G. Rumbles, C.-Z. Li, R. H. Friend,

- A. K.-Y. Jen and H. J. Snaith, *ACS Nano*, 2014, 8, 12701–12709.
- 13 J. Xu, A. Buin, A. H. Ip, W. Li, O. Voznyy, R. Comin, M. Yuan, S. Jeon, Z. Ning, J. J. McDowell, P. Kanjanaboos, J.-P. Sun, X. Lan, L. N. Quan, D. H. Kim, I. G. Hill, P. Maksymovych and E. H. Sargent, *Nat. Commun.*, 2015, 6, 7081.
- 14 Y. Shao, Z. Xiao, C. Bi, Y. Yuan and J. Huang, *Nat. Commun.*, 2014, 5, 5784.
- 15 J. Peng, Y. Wu, W. Ye, D. A. Jacobs, H. Shen, X. Fu, Y. Wan, T. Duong, N. Wu, C. Barugkin, H. T. Nguyen, D. Zhong, J. Li, T. Lu, Y. Liu, M. N. Lockrey, K. J. Weber, K. R. Catchpole and T. P. White, *Energy Environ. Sci.*, 2017, 10, 1792–1800.
- 16 H. Li, L. Tao, F. Huang, Q. Sun, X. Zhao, J. Han, Y. Shen and M. Wang, *ACS Appl. Mater. Interfaces*, 2017, 9, 38967–38976.
- 17 M. Abdi-Jalebi, Z. Andaji-Garmaroudi, S. Cacovich, C. Stavrakas, B. Philippe, J. M. Richter, M. Alsari, E. P. Booker, E. M. Hutter, A. J. Pearson, S. Lilliu, T. J. Savenije, H. Rensmo, G. Divitini, C. Ducati, R. H. Friend and S. D. Stranks, *Nature*, 2018, 555, 497–501.
- 18 X. Dong, H. Hu, B. Lin, J. Ding and N. Yuan, *Chem. Commun.*, 2014, 50, 14405–14408.
- 19 C. Y. Chang, K. T. Lee, W. K. Huang, H. Y. Siao and Y. C. Chang, *Chem. Mater.*, 2015, 27, 5122–5130.
- 20 A. Hultqvist, K. Aitola, K. Sveinbjörnsson, Z. Saki, F. Larsson, T. Törndahl, E. Johansson, G. Boschloo and M. Edoff, *ACS Appl. Mater. Interfaces*, 2017, 9, 29707–29716.
- 21 H. Si, Q. Liao, Z. Zhang, Y. Li, X. Yang, G. Zhang, Z. Kang and Y. Zhang, *Nano Energy*, 2016, 22, 223–231.
- 22 D. Koushik, W. J. H. Verhees, D. Zhang, Y. Kuang, S. Veenstra, M. Creatore and R. E. I. Schropp, *Adv. Mater. Interfaces*, 2017, 4, 1700043.
- 23 D. Koushik, W. J. H. Verhees, Y. Kuang, S. Veenstra, D. Zhang, M. A. Verheijen, M. Creatore and R. E. I. Schropp, *Energy Environ. Sci.*, 2017, 10, 91–100.
- 24 M. Kot, C. Das, Z. Wang, K. Henkel, Z. Rouissi, K. Wojciechowski, H. J. Snaith and D. Schmeisser, *ChemSusChem*, 2016, 9, 3401–3406.
- 25 G. W. P. Adhyaksa, L. W. Veldhuizen, Y. Kuang, S. Brittman, R. E. I. Schropp and E. C. Garnett, *Chem. Mater.*, 2016, 28, 5259–5263.
- 26 X. Dong, X. Fang, M. Lv, B. Lin, S. Zhang, J. Ding and N. Yuan, *J. Mater. Chem. A*, 2015, 3, 5360–5367.
- 27 V. Zardetto, B. L. Williams, A. Perrotta, F. Di Giacomo, M. A. Verheijen, R. Andriessen, W. M. M. Kessels and M. Creatore, *Sustainable Energy Fuels*, 2017, 1, 30–55.
- 28 Y. Li, F. Qian, J. Xiang and C. M. Lieber, *Mater. Today*, 2006, 9, 18–27.
- 29 E. C. Garnett, M. L. Brongersma, Y. Cui and M. D. McGehee, *Annu. Rev. Mater. Res.*, 2011, 41, 269–295.
- 30 L. Cao, J. S. White, J.-S. Park, J. A. Schuller, B. M. Clemens and M. L. Brongersma, *Nat. Mater.*, 2009, 8, 643–647.
- 31 F. Léonard, A. A. Talin, B. S. Swartzentruber and S. T. Picraux, *Phys. Rev. Lett.*, 2009, 102, 106805.
- 32 O. Demichel, V. Calvo, A. Besson, P. Noé, B. Salem, N. Pauc, F. Oehler, P. Gentile and N. Magnea, *Nano Lett.*, 2010, 10, 2323–2329.
- 33 Y. Dan, K. Seo, K. Takei, J. H. Meza, A. Javey and K. B. Crozier, *Nano Lett.*, 2011, 11, 2527–2532.
- 34 H. J. Joyce, J. Wong-Leung, C. K. Yong, C. J. Docherty, S. Paiman, Q. Gao, H. H. Tan, C. Jagadish, J. Lloyd-Hughes, L. M. Herz and M. B. Johnston, *Nano Lett.*, 2012, 12, 5325–5330.
- 35 E. Horváth, M. Spina, Z. Szekrényes, K. Kamarás, R. Gaal, D. Gachet and L. Forró, *Nano Lett.*, 2014, 14, 6761–6766.
- 36 J. Xing, X. F. Liu, Q. Zhang, S. T. Ha, Y. W. Yuan, C. Shen, T. C. Sum and Q. Xiong, *Nano Lett.*, 2015, 15, 4571–4577.
- 37 M. M. Tavakoli, A. Waleed, L. Gu, D. Zhang, R. Tavakoli, B. Lei, W. Su, F. Fang and Z. Fan, *Nanoscale*, 2017, 9, 5828–5834.
- 38 M. M. Tavakoli, K.-H. Tsui, S.-F. Leung, Q. Zhang, J. He, Y. Yao, D. Li and Z. Fan, *ACS Nano*, 2015, 150818123917002.
- 39 A. Waleed, M. M. Tavakoli, L. Gu, Z. Wang, D. Zhang, A. Manikandan, Q. Zhang, R.-J. Zhang, Y.-L. Chueh and Z. Fan, *Nano Lett.*, 2017, 17, 523–530.
- 40 L. Gu, M. M. Tavakoli, D. Zhang, Q. Zhang, A. Waleed, Y. Xiao, K.-H. Tsui, Y. Lin, L. Liao, J. Wang and Z. Fan, *Adv. Mater.*, 2016, 28, 9713–9721.
- 41 S. Z. Oener, P. Khoram, S. Brittman, S. A. Mann, Q. Zhang, Z. Fan, S. W. Boettcher and E. C. Garnett, *Nano Lett.*, 2017, 17, 6557–6563.
- 42 Y. Yang, Y. Yan, M. Yang, S. Choi, K. Zhu, J. M. Luther and M. C. Beard, *Nat. Commun.*, 2015, 6, 7961.
- 43 Y. Fang, Q. Dong, Y. Shao, Y. Yuan and J. Huang, *Nat. Photonics*, 2015, 9, 679–686.
- 44 B. Wu, H. T. Nguyen, Z. Ku, G. Han, D. Giovanni, N. Mathews, H. J. Fan and T. C. Sum, *Adv. Energy Mater.*, 2016, 6, 1–9.
- 45 L. M. Herz, *Annu. Rev. Phys. Chem.*, 2016, 67, 65–89.
- 46 Y. Yang, M. Yang, Z. Li, R. Crisp, K. Zhu and M. C. Beard, *J. Phys. Chem. Lett.*, 2015, 6, 4688–4692.
- 47 J. M. Richter, M. Abdi-Jalebi, A. Sadhanala, M. Tabachnyk, J. P. H. Rivett, L. M. Pazos-Outón, K. C. Gödel, M. Price, F. Deschler and R. H. Friend, *Nat. Commun.*, 2016, 7, 13941.
- 48 H. Wei, Y. Fang, P. Mulligan, W. Chuirazzi, H.-H. Fang, C. Wang, B. R. Ecker, Y. Gao, M. A. Loi, L. Cao and J. Huang, *Nat. Photonics*, 2016, 10, 333–339.
- 49 W. Yang, Y. Yao and C.-Q. Wu, *J. Appl. Phys.*, 2015, 117, 155504.
- 50 H.-H. Fang, S. Adjokatse, H. Wei, J. Yang, G. R. Blake, J. Huang, J. Even and M. A. Loi, *Sci. Adv.*, 2016, 2, e1600534.
- 51 G. W. P. Adhyaksa, S. Brittman, H. Ābolinš, A. Lof, X. Li, J. D. Keelor, Y. Luo, T. Duevski, R. M. A. Heeren, S. R. Ellis, D. P. Fenning and E. C. Garnett, *Understanding detrimental and beneficial grain boundary effects in halide perovskites*.
- 52 H.-H. Fang, R. Raissa, M. Abdu-Aguye, S. Adjokatse, G. R. Blake, J. Even and M. A. Loi, *Adv. Funct. Mater.*, 2015, 25, 2378–2385.